Re-entrant activity and its control in a model of mammalian ventricular tissue

Short title: *Model of ventricular re-entrant activity*

V.N. Biktashev[1,2] and A.V. Holden[2,*]

June 19, 1996

[1] *Institute for Mathematical Problems in Biology, Pushchino, Moscow Region, 142292, Russia*
[2] *Department of Physiology, University of Leeds, Leeds LS2 9JT, UK*
[*] *Author to whom correspondence should be addressed*

Abstract

We characterize the meander of re-entrant excitation in a model of a sheet of mammalian ventricular tissue, and its control by resonant drift under feedback driven stimulation. The Oxsoft equations for excitability in a guinea pig single ventricular cell were incorporated in a two dimensional reaction-diffusion system to model homogeneous, isotropic tissue with a plane wave conduction velocity of 0.7 m/s. Re-entrant spiral wave solutions have a spatially extended transient motion (linear core) that settles down into rotation with an irregular period of 100–110 ms around an irregular, multi-lobed spiky core. In anisotropic tissue this would appear as a linear conduction block. The typical velocity of drift of the spiral wave induced by low amplitude resonant forcing is 0.75 cm/s.

Keywords: arrhythmia, atrial flutter, re-entry, defibrillation, propagation, action potential

1 Introduction

Some cardiac arrhythmias are due to re-entrant propagation, in which the same wavefront repeatedly re-invades the same piece of tissue after propagating around an anatomical or functional block. Re-entrant spirals have been optically mapped in thin slices of epicardial tissue (Jalife & Davidenko 1993) and on the epicardial surface of the rabbit ventricle (Gray *et al.* 1995). The relatively thick wall of the ventricle means that propagation in ventricular muscle could be a predominantly three-dimensional phenomenon that occurs in an anisotropic and heterogeneous tissue, or could be explained by two-dimensional phenomena that result from the excitation properties rather than heterogeneity and anisotropy. In this paper we obtain the characteristics of re-entrant propagation in a two-dimensional, homogeneous model of ventricular tissue, and use these to account for the linear regions of unidirectional conduction blocks seen in mapping studies (Davidenko *et al.* , 1993), to explain why it is difficult to establish re-entrant propagation in the healthy ventricle, and to quantitatively assess low amplitude, repetitive stimulation by a spatially uniform electric field as a means of eliminating re-entry from ventricular tissue.

A spiral wave in a two-dimensional, homogeneous, isotropic excitable medium provides a model for re-entry. Spiral waves rotate around a central core, and may be characterized by their period of rotation, size of core, and movement of the tip of the spiral. At any specified instant in time a rotating spiral wave has a location, given by the position of its tip, and a spatial orientation of rotation phase.

A spiral wave can be forced to move by a spatially uniform, time periodic perturbation of appropriate frequency (Davydov *et al.* 1988). Resonant drift in the location of a spiral occurs when the frequency of perturbation is the same as the frequency of rotation of the spiral. In principle, resonant drift under feedback control could provide a means of eliminating re-entrant activity in cardiac tissue (Biktashev & Holden, 1994, 1995). This will be practical only if any re-entry is eliminated within a reasonable time, say less than 30 s, and so estimation of the velocities that can be achieved by resonant drift is important in assessing the feasibility of resonant drift as a means of controlling re-entrant arrhythmias.

We construct an excitable medium model for mammalian ventricular tissue by incorporating ordinary differential equations for ventricular cell excitability into a partial differential equation model. There are a number of models available for ventricular excitation that summarize the results of voltage clamp experiments — these include the Beeler-Reuter (1989) model, the Oxsoft guinea-pig ventricular cell model specified in (Noble 1991) and the phase 2 Luo-Rudy (1994) model. None of these models are definitive, they all represent steps in an on-going process of modelling the behaviour of ventricular cells by a description of membrane currents and pumps, and intracellular ion binding and concentration changes (Noble, 1995). Spiral waves solutions for rabbit atrial tissue models (Biktashev & Holden, 1995, and Winslow *et al.* 1995), show a reasonable agreement with experimental data. The Beeler-Reuter simplified ventricular model (Beeler & Reuter 1977) has been incorporated into two-dimensional tissue models, and reentrant solutions characterised by Courtemanche & Winfree (1991) and Efimov *et al.* (1995). Study of current ventricular models has been inhibited by the computational costs of this problem, which is a reflection of the stiffness of the kinetics of ventricular excitability.

In this paper we use equations of the Oxsoft guinea pig ventricle model. These equations provide a convenient starting point, as they have been extensively studied and give reasonable agreement with experiments. There are alternative approaches for description of mammalian ventricular cells, the most recent is that of Luo & Rudy (1994). A major problem with incorporating the Luo & Rudy (1994) 'phase two' model in two- and three-dimensional models of ventricular tissue is that the $[Ca^{++}]_i$ transient is triggered by $\partial V/\partial t_{\max}$ of the action potential, and during re-entry the action potential does not invade the core, $V(t)$ is slowed and almost constant close to the tip of the reentrant wave, and the behaviour near the tip determines meander, drift and stability of the re-entrant spiral wave.

The Oxsoft equations for cell excitability are incorporated into a reaction-diffusion equation with the voltage diffusion coefficient (hence, spatial scaling) selected to give an appropriate conduction velocity. Re-entrant spiral waves are initiated from a cut wavefront, or a twin-pulse protocol, and the evolution of their meander pattern followed. The velocity of resonant drift, produced by spatially uniform perturbations is obtained.

2 The numerical model

The Oxsoft equations (Noble 1990) for a single isopotential cell are in the form of a system of ordinary differential equations:

$$\begin{aligned} C\mathrm{d}V/\mathrm{d}t &= f(V,\mathbf{u}) \\ \mathrm{d}\mathbf{u}/\mathrm{d}t &= \mathbf{g}(V,\mathbf{u}), \end{aligned} \tag{1}$$

where C is the capacitance of a single cell, V the membrane potential in mV and $\mathbf{u}$ is a vector of the activation and inactivation gating variables and the ionic concentrations that determine the total membrane current $f(V,\mathbf{u})$. The full equations, together with the parameter values, are listed in the Appendix, and can also be obtained in the form of a Pascal program in Oxsoft HEART. This model was incorporated into a partial differential equation model for an excitable medium in the plane (x,y),

$$\begin{aligned} \partial V/\partial t &= C^{-1}f(V,\mathbf{u}) + D\nabla^2 V + F(t) \\ \partial \mathbf{u}/\partial t &= \mathbf{g}(V,\mathbf{u}), \end{aligned} \tag{2}$$

where D is the diffusion coefficient for V, ∇^2 is the Laplacian operator $(\partial^2/\partial x^2 + \partial^2/\partial y^2)$ and $F(t)$ is a spatially uniform, time dependent forcing that models external electric current applied to the tissue. The diffusion coefficient was chosen $D = 1.25\mathrm{cm}^2/\mathrm{s}$, which corresponds to intercellular (gap junction) resistance of $R = 250k\Omega$, by the formula $D(\mathrm{cell\,length})^{-2} = (RC)^{-1}$.

Calculations were performed using the explicit Euler method with five-node approximation of the Laplacian on a rectangular grid of 200×200 to 300×300 nodes with a time and space step of $h_t = 0.01$ms and $h_x = 0.2$mm (for the majority of experiments) or 0.001 ms and 0.1 mm (*i.e.* nearly the myocyte length) for a few control computations. Steps used in other published ventricular simulations were: 0.025 ms and 0.25 mm in (Courtemanche & Winfree 1991) and 0.1 ms and 0.25 mm in (Efimov *et al.* 1995).

The boundaries were modelled as impermeable,

$$\partial V/\partial x \mid_{x=x_{\min},x_{\max}} = \partial V/\partial y \mid_{y=y_{\min},y_{\max}} = 0, \tag{3}$$

with the medium large enough so that the exact form of boundary conditions does not influence the spiral wave behaviour.

At the space step of 0.2 mm, the upstroke velocity of the solitary wave was 570 V/s, and the conduction velocity (CV) 0.76 m/s; and at space step of 0.1 m/s, 500 V/s and 0.90 m/s correspondingly. Canine ventricular CV range from 0.14–0.25 m/s (transverse) to 0.5–0.8 m/s (longitudinal). The electrotonic space constant at the resting state is about 0.36 mm. Thus, the space step of 0.2 mm seems too large to get quantitatively exact results, as the error in important physiological quantities is up to 20%. The space step necessary for convergence of the CV estimate is less than cell size. As the space step is reduced, the CV with $D = 1.25\mathrm{cm}^2/\mathrm{s}$ converges to 0.97 m/s; the CV is within 5% of this 'true' value at $h_x = 0.05$mm *i.e.* less than the length of a single cell. However, the computed propagation patterns did not show the effects of anisotropy seen with coarse space steps, especially with the simplest Laplacian approximation we used, when grid geometry distorts curved wavefronts. The few methodological experiments we performed with the space step of 0.1 mm (computation cost grows as h_x^{-4} or even faster with account of overheads), did not show any significant change of the overall behaviour and so the simulation results should be correct, up to the value of diffusion coefficient or space scale.

The action of external forcing in the form of additive term $F(t)$ in (2) corresponds to injecting current into each cell and does not correspond to extracellular field stimulation. However, realistic models of external current require consideration of each cell as an extended object described by PDE, or at least integration of transmembrane currents over each cell's surface [13] and so massively increase the computational load. This paper is mostly concerned with the spontaneous evolution of spiral waves, and the qualitative features of resonant drift and so this simplification is acceptable. We measured the external forcing F in V/s in terms of its dimensionality in (2); this can easily be rescaled to amperes per cell by dividing by membrane capacitance C. The time dependent $F(t)$ used to produce resonant drift of the spiral wave was a series of rectangular pulses of 2 ms duration, applied at a fixed time after an action potential was detected at the recording site by V increasing through -10 mV.

Spiral waves were initiated in two ways, by a cut wavefront or twin pulse protocol. A plane wave was initiated at one edge of the medium by a 2 ms duration stimulation of a strip 1.3 mm wide, by a current that gave a $\mathrm{d}V/\mathrm{d}t$ of 50 V/s and the excitation allowed to propagate to the centre of the medium. The wavefront was then cut, and all the variables on one side of the cut reset to their equilibrium values. This numerically convenient but artificial method allows spirals to be initiated in a 4×4 cm medium. The twin pulse protocol requires a larger (6×6 cm) medium, in which a plane wave is initiated at the lower border by 10 ms stimulation of 50 V/s of a two mm strip, and 180 ms later (after the wavefront has propagated through the medium, establishing a

gradient in refractoriness) the second stimulus is applied: a 4 ms stimulation of 40 V/s over the left 6×5 cm area of the medium. These large area (larger than endocardial surface of a rabbit atrium) are necessary for the initiation of reentry in a homogeneous tissue; re-entry persists in smaller media, see Fig. 1.

By anisotropic medium we understood (2) with Laplacian replaced by $(\delta\partial^2/\partial x^2 + \partial^2/\partial y^2)$ or $(\partial^2/\partial x^2 + \delta\partial^2/\partial y^2)$ with $\delta = 1/9$, which is equivalent to 3-fold compression in x or y direction, respectively.

Simulating 1 s of activity in a 4×4 cm medium with $\Delta t = 0.01$ms and $\Delta x = 0.2$mm took about 180 hours on a single MIPS R8000 75 MHz central processor unit.

3 Results

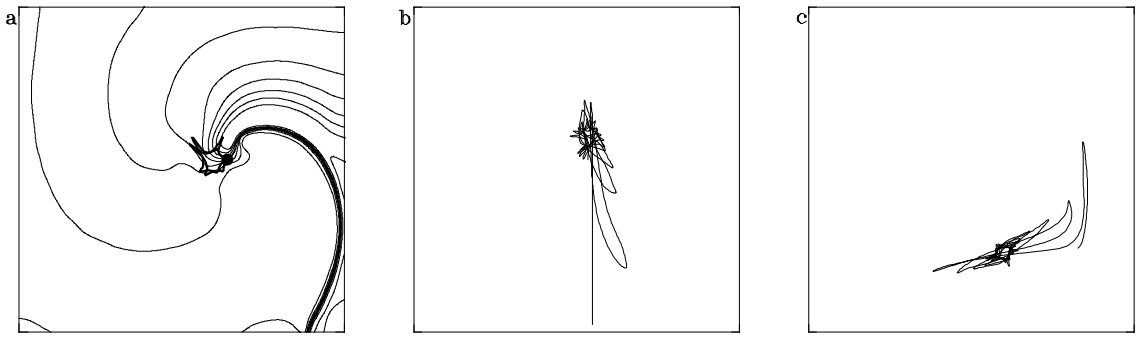

Figure 1: (a) Isopotential map and tip trajectory of spiral wave solution of equations (2) and (3), in a 40×40 mm medium with $h_t = 0.01$ms and $h_x = 0.2$mm, with the 10 voltage isolines spanning -89.4 to 32.4 mV in equal steps of 13.5 mV. The isolines represent the $V(t)$ waveform 2.67 s after its initiation from a broken wavefront, and the solid line ending in • is the trajectory of the tip during the preceding 190 ms. (b, c) The tip trajectory for spiral wave solutions of (2, 3) produced by a cut plane wave (b) and a twin stimulus protocol (c).

Figure 1(a) illustrates a spiral wave solution of the model, as the spatial distribution of isolines of membrane potential V, at an instant 2.67 s after the spiral wave was initiated by cutting a broken plane wave. The spiral rotated with an initial period of approximately 170 ms, and over the first 1 s the period decreased to 100–110 ms. If the medium were large enough, the distance between successive wavefronts far from the tip, *i.e.* the wavelength of the spiral would be about 8 cm. We define the tip of the spiral by the intersection of the $V = -10\ mV$ and the $f = 0.5$ isolines, where f is the Ca^{++} inactivation gating variable. The qualitative behaviour of the trajectory of the tip does not depend on the precise choice of these values. The trajectory of the tip of the spiral is not stationary, but meanders, and its motion is nonuniform, moving by a jump-like alternation between fast and very slow phases, with about 5 jumps per full rotation. This motion resembles an irregular, nearly biperiodic process, with the ratio of the two periods close to 1:5.

The multi-lobed pattern of the trajectory of the tip takes time to develop, and itself develops with time. Figure 1(b,c) follows the tip trajectory for spirals initiated from a broken wavefront (b), by a twin pulse protocol (c). In both cases the tip trajectory follows a transient over 3–4 rotations, in which there is an extended "core", with a length of some centimeters, that evolves into an irregular, biperiodic motion around a core contained within 7 mm square. Both the extended transient and the biperiodic motions are composed of almost linear segments (when the velocity of the tip movement is fast, about 0.3 m/s) broken by sharp turns of up to 170° (when the tip trajectory is almost stationary).

The rotation of the spiral wave can be monitored by following an isoline on the wavefront, and the trajectory of the tip of the spiral, as illustrated in Figure 2(a). The area enclosed by the tip trajectory is analogous to the core of a rigidly rotating spiral, and is not invaded by the action potential. Characteristics of the $V(t)$ observed at different sites in the medium during the evolution of a rotating spiral wave are (Figure 2(b))

- only the first action potential, produced by activity invading a resting medium, has the fast depolarization and overshoot that are characteristic of solitary membrane action potential solutions of (1),
- far from the tip of the spiral wave, the repetitive action potentials are faster and larger than closer to the tip, and have an amplitude and shape determined by their rate (of about 10 s^{-1}),

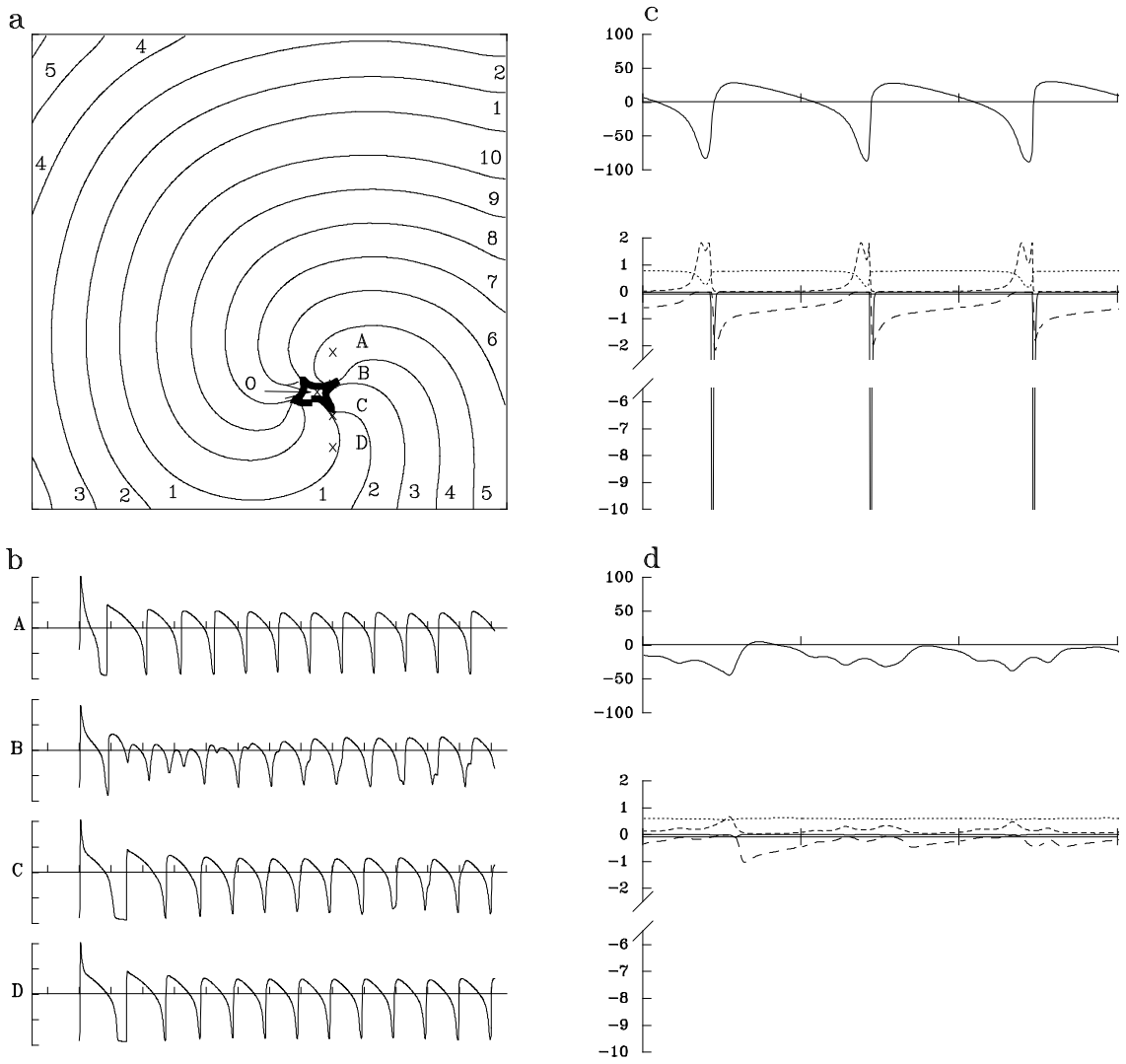

Figure 2: (*a*) Isochronal map of a spiral wave solution of equations (2) and (3), initiated by the twin pulse protocol in a 60×60 mm medium with $h_t = 0.05$ ms and $h_x = 0.2$ mm. Thin lines are the excitation front position, drawn at every 10 ms during one rotation 1.2 to 1.29s. The front lines are defined as loci of $V = -25$mV and $f > 0.5$, where f is the Ca^{++} inactivation gating variable. The thick line is the trajectory of the spiral tip during this rotation. *A–D* and *O* mark the position of recording sites. (*b*) $V(t)$ at sites *A–D* during the first 12 rotations of the spiral after its initiation. Voltage scale is from -100 mV to 100 mV with marks in 50 mV, marks on time axis are in 100 ms. (*c,d*) Membrane potential $V(t)$, upper graphs, and principal currents i_{Na} (solid), i_{Ca} (long dashed), i_{K_1} (medium dashed), i_K (dotted), lower graphs, at points *A* (*c*) and *O* (*d*) of Figure 2(*a*), 1.5 to 1.8 s after the initiation of spiral wave from broken wavefront. Voltage is in mV, current in nA, marks on time axis through 100 ms.

- close to the tip both the amplitude and $\partial V/\partial t_{\max}$ are reduced by more than an order of magnitude, and $V(t)$ appears more as slow oscillations than action potentials.

The membrane potential and principal currents (i_{Na}, i_{Ca}, i_{K_1}, i_K) far from, and within the core of the spiral, sites *"A"* and *"O"* of Figure 2(*a*), are illustrated in Figure 2(*c,d*), respectively. Within the core (d) the membrane potential remains between -45 and -5 mV; this persistent depolarization inactivates the inward current i_{Na} (on the graph, it is indistinguishable from zero), thus blocking propagation into the core. The trajectory of the tip maps out an area of the conduction block. Note that the change of action potential waveform in different sites is a general feature of spiral waves in excitable media; see *e.g.* (Plesser *et al.* 1990) for analogous waveform changes in the Belousov-Zhabotinsky reaction.

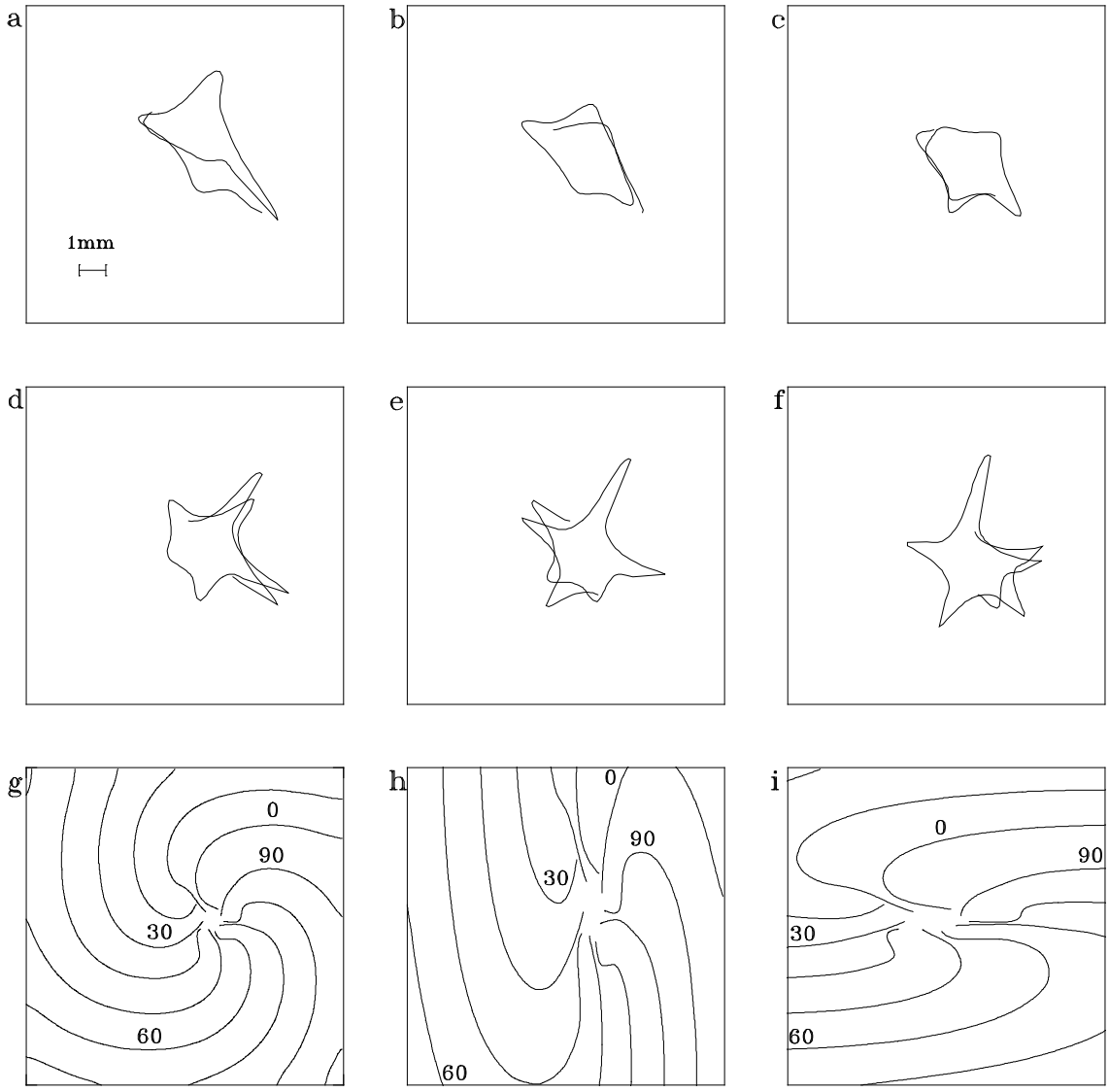

Figure 3: (*a–f*) Successive 150 ms pieces of the tip trajectory, starting 1.5 s after spiral initiation from a broken plane wave, with $h_x = 0.2$mm, $h_t = 0.01$ms, in a medium 40×40 mm. (*g–i*) Isochronal map during of biperiodic tip meander, 2.480–2.520 s since spiral was initiated from a broken plane wave, (*g*) in isotropic medium, (*h*) in anisotropic medium with longitudinal axis of fibres in the vertical direction, and (*i*) in anisotopic medium, with longitudinal axis of fibres in the horizontal direction. The isochrons are labeled in ms relative to 2480 ms. $h_t = 0.01$ms, $h_x = 0.2$mm, medium 40×40 mm.

Figure 3(*a–f*) shows that as the asymmetric, multilobed trajectory continues to evolve, the area it encloses continues to decrease, and the pattern changes from having two or three sharp turns, to having five. The trajectory during any rotation differs from the trajectory during the preceding rotations. The spiral wave solutions have been followed for up to 3 s, and so, once established, the slowly evolving, almost biperiodic meander pattern shown in Figures 1–3 appears to be stable.

Anisotropy in conduction velocity will distort the spiral wave and tip trajectory; Figure 3(*g–i*) shows voltage isochrons in isotropic and anisotropic media: in the isotropic medium the isochrons

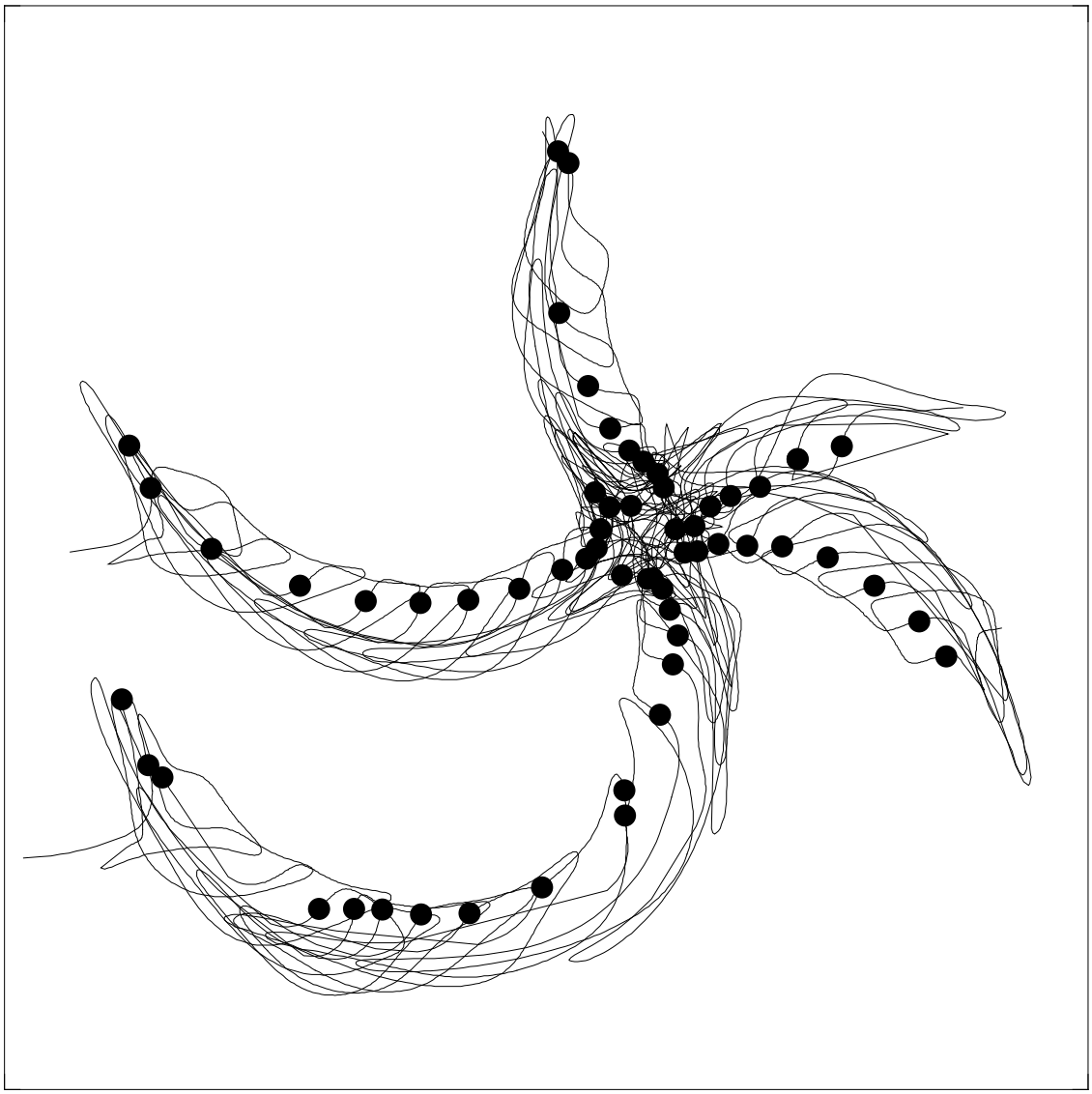

Figure 4: Tip trajectories under feedback controlled, resonant driving. When the wavefront of the spiral wave (depolarization through -10 mV) reached a recording site in the bottom left hand corner, a 2 ms, 4 V/s depolarizing perturbation was added after a fixed delay. Each trajectory is for a different delay, from 0 to 100 ms, and corresponds to applying the perturbation at a different phase of the spiral. All trajectories start in the same place in the center, move toward boundaries and annihilate. The dots mark point on trajectories corresponding to the moments of stimulation.

for the small, multilobed tip trajectory of Figure 3(*a–f*) appear to emerge from a compact core, while in the anisotropic medium the isochrons appear to move around a linear core.

The tip of the spiral wave solutions of Figures 1–3 moves irregularly in a complicated trajectory, but does not move out of the medium: if the medium is large enough to contain the early transient motion around an almost linear core then the spiral wave remains in the medium. Small amplitude, spatially uniform repetitive stimulation under feedback control can be used to produce directed movement of a rigidly rotating spiral wave and so to push the spiral out the medium (Biktashev & Holden, 1994). Figure 4 shows five tip trajectories produced by repetitive stimulation applied at five different fixed delays after the wavefront reached the bottom left hand corner of the medium. The delay determines the initial direction of drift. The curved drift trajectories all reach the medium boundaries. A repetitive perturbation of 15% the amplitude of the single shock defibrillation threshold produces a directed motion with a velocity of about 0.75 cm/s. Here we mean by defibrillation threshold the minimal amplitude of a brief pulse $F(t)$ in (2), which is sufficient to eliminate the re-entrant activity, about 12.5 V/s.

4 Discussion

The relevance of these computations to propagation during re-entrant arrhythmias in ventricular tissue can be assessed by quantitative features of the re-entry — the period and waveform of the action potential, the size of the medium within which re-entry can be initiated, the rapidly decaying transient and then slow ageing of the re-entrant wave (i.e. change of period and core shape due to slow processes), the irregular, jump-like motion of the re-entrant wave, and the velocity at which it can be moved by resonant perturbation. The relevance can be questioned, on the grounds that macro- and micro-anatomical detail is ignored, as are the effects of heterogeneity. We would argue that the reasonable correspondence between the computations and observations of re-entrant propagation means that cardiac tissue, in spite of its cellularity, three-dimensional anatomy and heterogeneity, behaves as a reaction diffusion system, and so methods for controlling spiral waves in such systems may be applicable to controlling propagation during re-entrant ventricular arrhythmias.

Although $\partial V/\partial t_{\max}$ of a solitary action potential of the single cell model (580 V/s) compares well with the values of 512 ± 68 V/s obtained by Taniguchi *et al.* (1994) for guinea-pig isolated ventricular myocytes, the computed value of $\partial V/\partial t_{\max}$ for the propagating wavefronts are too high. Taniguchi *et al.* obtained $\partial V/\partial t_{\max}$ for propagating action potentials as 231 ± 35 V/s (longitudinal propagation) and 309 ± 33 V/s (transverse propagation). The difference in transverse and longitudinal $\partial V/\partial t_{\max}$ correlates with the anistropy in conduction velocity; the longitudinal space constant is longer than the transverse space constant, and so inward membrane current depolarises the capacitance of tissue further ahead in the longitudinal than transverse direction. The slow down of $\partial V/\partial t_{\max}$ is partly due to the increase in capacitative load, and partly due to a slow inactivation of the Na conductance by electrotonic current. Both effects are seen in the computations with the Oxsoft model, but the maximal effect (produced in the limit $R = 0$) is only a 30% reduction in $\partial V/\partial t_{\max}$. Thus the unreasonably fast $\partial V/\partial t_{\max}$ is due to a mismatch in behaviour of the Na system between the model and ventricular cells.

The period of the spiral wave of about 100–110 ms in our model corresponds to 120–240 ms in the human, 110–165 ms in the rabbit, 120–130 ms in the pig *in situ*, 120–250 ms in the sheep and 100–200 ms in the dog for epicardial tissue slices (Pertsov *et al.* 1993). Computations by Courtemanche & Winfree (1991) with the modified Beeler-Reuter model give a longer (190–300 ms) period.

The persistence of the spiral wave solution (*i.e.* their stability and lack of breakdown) is consistent with the experimental observations of Davidenko *et al.* (1993). The earlier computations of Panfilov & Holden (1990) for a Purkinje-fibre kinetics and Courtemanch & Winfree (1991) for Beeler-Reuter kinetics showed spontaneous spiral breakdown.

The transient, extended tip trajectories seen on initiating a spiral wave in Figure 1(b,c) means that although a large medium is required to initiate a re-entrant wave, once established, it can survive in a smaller medium. A transient change in medium properties (say, a decrease in action potential duration produced by a transient ischaemic episode) could allow the creation of re-entry in the transient abnormal tissue, and this could persist even when the tissue properties returned to normal, even though the size of the tissue was smaller than the critical mass (Zipes *et al.* 1975).

The slow ageing, i.e. change of the re-entry features from one period to another, is analogous to that seen in atrial tissue models (Holden & Zhang, 1995), in that it is due to the slow dynamics of some of the current, pump and concentration components. However, the key characteristic of meander in this ventricular model is the alternation between fast, almost linear, motions and slow, sharp turns. This gives a core with a large perimeter but small area, and results from the dynamic interplay between the fast rate of the action potential depolarization forcing high curvature, while the long duration of the action potential only allows small curvatures. This provides a general mechanism for 'linear' conduction blocks in homogeneous excitable media with ventricular-like action potentials. This correlates with 'linear', 'Z-shaped' and 'hypocycloidal' conduction blocks observed in cellular automata (Fast *et al.* 1990), modified FitzHugh-Nagumo (Krinsky *et al.* 1992) and Beeler-Reuter (Efimov *et al.* 1995) media. For instance, a 'Z-shaped' core is similar to trajectory observed in first couple of rotations in our simulations. These extended arcs of conduction block would be enhanced by anisotropy in conduction velocity, as seen in Figure 3(h,i) as 'linear conduction block'.

A re-entrant wave in such an anisotropic circuit can have an excitable gap (in which recovery of excitability has occured) before the tissue is re-excited by the re-entrant wave. During the slow, sharp turn, the gap ahead is large; during the faster, linear motion the gap is smaller. However, in any case the excitable gap anywhere far from the core is virtually absent (see Fig. 2(b,c)).

We have proposed resonant drift under feedback control as a means of defibrillating cardiac (Biktashev & Holden 1994) and atrial (Biktashev & Holden 1995) tissues. This method exploits the stability and symmetry of a rigidly rotating spiral (*i.e.* with a circular core): the key idea is

that stable spiral waves can be displaced by spatially uniform perturbations, and so appropriately timed perturbations could be used to drive a spiral wave out of a medium. The nonuniform tip velocity, and the spiky pattern of meander, both complicate the response of the ventricular model spiral wave to perturbation. The trajectories obtained by feedback controlled, resonant driving of the position of the spiral wave solution shown in Figure 4 show that resonant drift can be used to control the position of reentrant sources in this model, and so feedback controlled resonant drift of re-entrant activity of a free (unpinned) spiral or scroll wave may be produced in ventricular tissue. However, even in two-dimensional tissue slices, the effects of local heterogeneities, that pin or bind re-entrant sources, may be dominant (Vinson *et al.* 1994).

In summary, a two-dimensional partial differential equation model of ventricular tissue, with a detailed description of membrane excitability, generates persistent re-entrant waves with an appropriate waveform and period, and with extended cores that would be apparent in mapping studies as lines or arcs of unidirectional conduction block. These re-entrant waves can be moved by resonant drift , with a velocity that would force a re-entrant wave to a medium boundary in an epicardial tissue slice preparation within 10 s, if the re-entry was not trapped by localized heterogeneities. Resonant drift under feedback control can be used to move re-entrant sources even when their pattern of rotation is not a rigid rotation around a circular core, but is around a line or arc of unidirectional conduction block.

5 Acknowledgments

This work was partly funded by a visiting fellowship from The Wellcome Trust (038817) and grants from the Russian Fund for Basic Research (93-011-16080, 96-01-00592), EPSRC (GR/K/49775) and the Wellcome Trust (044365)

References

[1] Beeler, G. & Reuter, H. 1989 Reconstruction of the action potential of ventricular myocardial fibres *J. Physiol. (Lond)* **268,** 963–977.

[2] Biktashev, V.N. & Holden, A.V. 1994 Design principles for a low voltage cardiac defibrillator based on the effect of feedback resonant drift *J. Theor. Biol.* **169,** 101–112.

[3] Biktashev, V.N. & Holden, A.V. 1995 Control of reentrant activity in a model of mammalian atrial tissue *Proc. Roy. Soc.* **B260,** 211–217.

[4] Courtemanche, M. & Winfree, A.T. 1991 Re-entrant rotating waves in a Beeler-Reuter based model of two-dimensional cardiac electrical activity *Int. J. Bifurcation & Chaos* **1,** 431–444.

[5] Davidenko, J.M., Kent, P.F. & Jalife, J. 1993 Spiral waves in normal isolated ventricular muscle *Physica D* **49,** 182–197.

[6] Davydov, V.A., Zykov, V.S., Mikhailov, A.S. & Brazhnik, P.K. 1988 Drift and resonance of spiral waves in active media *Izv. VUZov — Radiofizika / Sov. Phys. — Radiophysics* **31**, 574–582.

[7] Efimov, I.R., Krinsky, V.I. & Jalife, J. 1995 Dynamics of rotating vortices in the Beeler-Reuter model of cardiac tissue *Chaos, Solitons and Fractals* **5,** 513–526.

[8] Fast, V.G., Efimov, I.R. & Krinsky, V.I. "Transition from circular to linear rotation of a vortex in an excitable cellular medium" Phys. Letters A **151**, 157–161

[9] Fast, V.G. & Pertsov, A.M. 1992 "Shift and termination of functional reentry in isolated ventricular preparations with quinidine-induced inhomogeneity in refractory period", *J. Cardiovasc. Electrophysiology* **3**, 255–265

[10] Gray, R.A., Jalife, J., Panfilov, A.V., Baxter, W.T., Cabo, C., Davidenko, J.M., Pertsov, A.M 1995 Mechanisms of Cardiac Fibrillation *Science* **270**, 1222–1223.

[11] Holden, A.V. & Zhang, H. 1995 Characteristics of atrial re-entry and meander computed from a model of a rabbit single atrial cell *J. Theor. Biol.* **175,** 545–551.

[12] Jalife, J. & Davidenko, J.M. 1993 Spiral waves as a mechanism of reentrant excitation in isolated cardiac muscle. In *Cardiac Mapping* (ed. M. Shenasa, M. Borggrefe and G.Breithardt), pp. 607-623, Mount Kisco, NY: Futura Pub Co.

[13] Krassowska W. & Neu J.C. "Response of a single cell to an external electric field", *Biophysical Journal* **66**: 1768–1776

[14] Krinsky, V.I., Efimov, I.R. & Jalife, J. 1992 Vortices with linear cores in excitable media *Proc. Roy. Soc. Lond.* **A43, 7** 645–655.

[15] Luo, C.H., Rudy, Y. 1994 A dynamic model of the cardiac ventricular action-potential I&II *Circ. Res.* **74,** 1071–1096, 1097–1113.

[16] Noble, D. 1990 *Oxsoft HEART Version 3.8 manual.* Oxford: Oxsoft.

[17] Noble, D. 1995 The development of mathematical models of the heart *Chaos Solitons and Fractals* **5,** 321–333.

[18] Panfilov, A.V. & Holden, A.V. 1990 "Self-generation of turbulent vortices in a 2-dimensional model of cardiac tissue", Phys. Letters A, **151**, 23-26

[19] Pertsov, A.M., Davidenko, J.M., Salmonsz, R., Baxter, W.T. & Jalife J. 1993 Spiral waves of excitation underlie reentrant activity in isolated cardiac muscle *Circ. Res.* **72,** 631–650.

[20] Plesser T., Müller S.C. & Hess B. 1990 "Spiral wave dynamics as a function of proton concentration in the ferroin-catalyzed Belousov-Zhabodinsky reaction", *J. Phys. Chem* **94**, 7501–7507

[21] Taniguchi, A., Toyama, J., Kodama, I., Anno,T., Shirakawa, M. & Usui, S. 1994 Inhomogeneity of cellular activation time and Vmax in normal myocardial tissue under electrical field stimulation. *Am. J. Physiol* **276** *Heart Circ. Physiol.* **36** H694-H705.

[22] Vinson, M., Pertsov, A. & Jalife, J. 1994 Anchoring of vortex filaments in 3D excitable media *Physica D* **72,** 119–134.

[23] Zipes, D.P., Fischer, J., King, R.M. *et al.* 1975 Termination of ventricular fibrillation in dogs by depolarizing a critical amount of myocardium *Am. J. Cardiol.* **36,** 37–44.

A Appendix. Equations of Excitability of a Single Guinea Pig Ventricular Cell

A.1 Units

s	second	time
μm	micrometer	space
μl	microlitre	volume
mJ	millijoule	energy
C	coulomb	electric charge
mV	millivolt	potential
nA	nanoampere	current
°K	kelvin	temperature
μS	microsiemen	conductance
μF	microfarad	capacitance
mol	mole	amount of substance
mM	mole per litre	concentration

A.2 Independent Dynamic Variables

- V - transmembrane voltage, mV
- m, h, d, x, f, q, r, f_{act}, f_{prod} - gating variables, $0 \ldots 1$
- $[Na^+]_{\mathrm{i}}$, $[K^+]_{\mathrm{i}}$, $[Ca^{2+}]_{\mathrm{i}}$ - intracellular ion concentrations, mM
- $[Ca^{2+}]_{\mathrm{up}}$, $[Ca^{2+}]_{\mathrm{rel}}$, $[Ca^{2+}]_{\mathrm{calmod}}$, $[Ca^{2+}]_{\mathrm{trop}}$ - intracellular partial $[Ca^{2+}]$ concentrations, mM

A.3 Differential equations

$$
\begin{aligned}
\dot{V} &= \frac{-1}{C}(I_{\mathrm{K}} + I_{\mathrm{K1}} + I_{\mathrm{to}} + I_{\mathrm{siK}} + I_{\mathrm{bK}} + I_{\mathrm{NaK}} + I_{\mathrm{Na}} + I_{\mathrm{bNa}} + \\
&\quad I_{\mathrm{siNa}} + I_{\mathrm{NaCa}} + I_{\mathrm{siCa}} + I_{\mathrm{bCa}}) \\
\dot{m} &= \frac{200(V+41)}{1-e^{-0.1(V+41)}}(1-m) - 8000e^{-0.056(V+66)}m \\
\dot{h} &= 20e^{-0.125(V+75)}(1-h) - \frac{2000}{1+320e^{-0.1(V+75)}}h \\
\dot{d} &= \frac{90(V+19)}{1-e^{-(V+19)/4}}(1-d) - \frac{36(V+19)}{e^{(V+19)/10}-1}d \\
\dot{x} &= \frac{0.5e^{0.0826(V+50)}}{1+e^{0.057(V+50)}}(1-x) - \frac{1.3e^{-0.06(V+20)}}{1+e^{-0.04(V+20)}}x \\
\dot{f} &= \frac{3.125(V+34)}{e^{(V+34)/4}-1}(1-f) - \frac{25}{1+e^{-(V+34)/4}}f \\
\dot{q} &= 333(\frac{1}{1+e^{-(V+4)/5}} - q) \\
\dot{r} &= 0.033e^{-V/17}(1-r) - \frac{33}{1+e^{-(V+10)/8}}r \\
\dot{[Na^+]}_{\mathrm{i}} &= \frac{-1}{V_{\mathrm{i}}F}(I_{\mathrm{Na}} + I_{\mathrm{bNa}}\frac{[Na^+]_{\mathrm{o}}}{140} + 3I_{\mathrm{NaK}} + 3I_{\mathrm{NaCa}} + I_{\mathrm{siNa}}) \\
\dot{[K^+]}_{\mathrm{i}} &= \frac{-1}{V_{\mathrm{i}}F}(I_{\mathrm{K}} + I_{\mathrm{K1}} + I_{\mathrm{siK}} + I_{\mathrm{bK}} + I_{\mathrm{to}} - 2I_{\mathrm{NaK}}) \\
\dot{[Ca^{2+}]}_{\mathrm{i}} &= \frac{-1}{2V_{\mathrm{i}}F}(I_{\mathrm{siCa}} + I_{\mathrm{bCa}} - 2I_{\mathrm{NaCa}}) - I_{\mathrm{up}} + I_{\mathrm{rel}}\frac{V_{\mathrm{SRup}}V_{\mathrm{rel}}}{V_{\mathrm{i}}V_{\mathrm{up}}} \\
&\quad -\dot{[Ca^{2+}]}_{\mathrm{calmod}} - \dot{[Ca^{2+}]}_{\mathrm{trop}} \\
\dot{[Ca^{2+}]}_{\mathrm{up}} &= \frac{V_{\mathrm{i}}}{V_{\mathrm{SRup}}}I_{\mathrm{up}} - I_{\mathrm{tr}} \\
\dot{[Ca^{2+}]}_{\mathrm{rel}} &= \frac{V_{\mathrm{up}}}{V_{\mathrm{rel}}}I_{\mathrm{tr}} - I_{\mathrm{rel}} \\
\dot{[Ca^{2+}]}_{\mathrm{calmod}} &= 10^5(M_{\mathrm{trop}} - [Ca^{2+}]_{\mathrm{calmod}})[Ca^{2+}]_{\mathrm{i}} - 50[Ca^{2+}]_{\mathrm{calmod}}
\end{aligned}
$$

$$
\begin{aligned}
\dot{[Ca^{2+}]}_{\mathrm{trop}} &= 10^5(C_{\mathrm{trop}} - [Ca^{2+}]_{\mathrm{trop}})[Ca^{2+}]_{\mathrm{i}} - 200[Ca^{2+}]_{\mathrm{trop}} \\
\dot{f}_{\mathrm{act}} &= (1 - f_{\mathrm{act}} - f_{\mathrm{prod}})(500(\frac{[Ca^{2+}]_{\mathrm{i}}}{[Ca^{2+}]_{\mathrm{i}} + k_{\mathrm{mCa}}})^2) \\
&\quad -f_{\mathrm{act}}(500(\frac{[Ca^{2+}]_{\mathrm{i}}}{[Ca^{2+}]_{\mathrm{i}} + k_{\mathrm{mCa}}})^2 + 60) \\
\dot{f}_{\mathrm{prod}} &= f_{\mathrm{act}}(500(\frac{[Ca^{2+}]_{\mathrm{i}}}{[Ca^{2+}]_{\mathrm{i}} + k_{\mathrm{mCa}}})^2 + 60) - f_{\mathrm{prod}}
\end{aligned}
$$

A.4 Dependent Quantities - Functions of Dynamic Variables

A.4.1 Channel Transmembrane Currents

$$
\begin{aligned}
I_{\mathrm{K}} &= \frac{xI_{\mathrm{Kmax}}}{140}([K^+]_{\mathrm{i}} - [K^+]_{\mathrm{o}}e^{\frac{-V}{RT/F}}) \\
I_{\mathrm{K1}} &= G_{\mathrm{K1}}\frac{[K^+]_{\mathrm{o}}}{[K^+]_{\mathrm{o}} + k_{\mathrm{mK1}}}(\frac{V - E_{\mathrm{K}}}{1 + e^{\frac{V - E_{\mathrm{K}} + 10 - V_{\mathrm{shift}}}{RT/2F}}}) \\
I_{\mathrm{to}} &= G_{\mathrm{to}}(V - E_{\mathrm{K}})qr \\
I_{\mathrm{bK}} &= G_{\mathrm{bK}}(V - E_{\mathrm{K}}) \\
I_{\mathrm{Na}} &= G_{\mathrm{Na}}(V - E_{\mathrm{mh}})m^3h \\
I_{\mathrm{bNa}} &= G_{\mathrm{bNa}}(V - E_{\mathrm{Na}}) \\
I_{\mathrm{siCa}} &= 4P_{\mathrm{Ca}}df\frac{\frac{V-50}{RT/F}}{1 - e^{\frac{-(V-50)}{RT/2F}}}[[Ca^{2+}]_{\mathrm{i}}e^{\frac{50}{RT/2F}} - [Ca^{2+}]_{\mathrm{o}}e^{\frac{-(V-50)}{RT/2F}}] \\
I_{\mathrm{siK}} &= P_{\mathrm{CaK}}P_{\mathrm{Ca}}df\frac{\frac{V-50}{RT/F}}{1 - e^{\frac{-(V-50)}{RT/F}}} \\
&\quad [[K^+]_{\mathrm{i}}e^{\frac{50}{RT/F}} - [K^+]_{\mathrm{o}}e^{\frac{-(V-50)}{RT/F}}] \\
I_{\mathrm{siNa}} &= P_{\mathrm{CaNa}}P_{\mathrm{Ca}}df\frac{\frac{V-50}{RT/F}}{1 - e^{\frac{-(V-50)}{RT/F}}} \\
&\quad [[Na^+]_{\mathrm{i}}e^{\frac{50}{RT/F}} - [Na^+]_{\mathrm{o}}e^{\frac{-(V-50)}{RT/F}}] \\
I_{\mathrm{bCa}} &= G_{\mathrm{bCa}}(V - E_{\mathrm{Ca}})
\end{aligned}
$$

A.4.2 Pump/Exchanger Transmembrane Currents

$$
\begin{aligned}
I_{\mathrm{NaK}} &= I_{\mathrm{NaKmax}}\frac{[K^+]_{\mathrm{o}}}{[K^+]_{\mathrm{o}} + k_{\mathrm{mK}}}\frac{[Na^+]_{\mathrm{i}}}{[Na^+]_{\mathrm{i}} + k_{\mathrm{mNa}}} \\
I_{\mathrm{NaCa}} &= k_{\mathrm{NaCa}}\frac{e^{\gamma\frac{V}{RT/F}}[Na^+]_{\mathrm{i}}{}^3[Ca^{2+}]_{\mathrm{o}} - e^{-(1-\gamma)\frac{V}{RT/F}}[Na^+]_{\mathrm{o}}^3[Ca^{2+}]_{\mathrm{i}}}{1 + d_{\mathrm{NaCa}}([Ca^{2+}]_{\mathrm{i}}[Na^+]_{\mathrm{o}}{}^3 + [Ca^{2+}]_{\mathrm{o}}[Na^+]_{\mathrm{i}}{}^3)}
\end{aligned}
$$

A.4.3 $[Ca^{2+}]$ Sequestration Flows

$$
\begin{aligned}
I_{\mathrm{up}} &= \frac{3.0[Ca^{2+}]_{\mathrm{i}} - 0.23[Ca^{2+}]_{\mathrm{up}}\frac{k_{\mathrm{cyca}}k_{\mathrm{xcs}}}{k_{\mathrm{srca}}}}{[Ca^{2+}]_{\mathrm{i}} + [Ca^{2+}]_{\mathrm{up}}\frac{k_{\mathrm{cyca}}k_{\mathrm{xcs}}}{k_{\mathrm{srca}}} + k_{\mathrm{cyca}}k_{\mathrm{xcs}} + k_{\mathrm{cyca}}} \\
I_{\mathrm{tr}} &= 50([Ca^{2+}]_{\mathrm{up}} - [Ca^{2+}]_{\mathrm{rel}}) \\
I_{\mathrm{rel}} &= (\frac{f_{\mathrm{act}}}{f_{\mathrm{act}} + 0.25})^2 k_{\mathrm{mCa2}}[Ca^{2+}]_{\mathrm{rel}}
\end{aligned}
$$

A.4.4 Reversal potentials

$$
E_{\mathrm{Na}} = \frac{RT}{F}\log(\frac{[Na^+]_{\mathrm{o}}}{[Na^+]_{\mathrm{i}}})
$$

$$
\begin{aligned}
E_{\mathrm{K}} &= \frac{RT}{F}\log(\frac{[K^+]_{\mathrm{o}}}{[K^+]_{\mathrm{i}}}) \\
E_{\mathrm{Ca}} &= \frac{RT}{2F}\log(\frac{[Ca^{2+}]_{\mathrm{o}}}{[Ca^{2+}]_{\mathrm{i}}}) \\
E_{\mathrm{mh}} &= \frac{RT}{F}\log(\frac{[Na^+]_{\mathrm{o}} + 0.12[K^+]_{\mathrm{o}}}{[Na^+]_{\mathrm{i}} + 0.12[K^+]_{\mathrm{i}}})
\end{aligned}
$$

A.5 Standard Parameter Values

C	$200 \cdot 10^{-6}\mu$F	k_{NaCa}	$5 \cdot 10^{-4} nA$
I_{Kmax}	1.0nA	d_{NaCa}	0.0
k_{mK1}	10mM	γ	$\frac{1}{2}$
k_{mK}	1mM	k_{cyca}	$3 \cdot 10^{-4}$mM
k_{mNa}	40mM	k_{xcs}	0.4mM
k_{mCa}	$7 \cdot 10^{-4}$mM	k_{srca}	0.5mM
V_{shift}	20.0mV	F	96485C/mol
I_{NaKmax}	0.7nA	R	8314.41mJ/(mol°K)
G_{Na}	2.5μS	T	310°K
G_{to}	0.005μS	V_{ecs}	0.4
G_{bK}	$.0006\mu$S	$radius$	15μm
G_{K1}	1.0μS	$length$	80μm
G_{bNa}	$.0006\mu$S	V_{cell}	$\cdot 10^{-9}\pi\ radius^2 length, \mu$l
G_{bCa}	$.00025\mu$S	V_{i}	$(1 - V_{\mathrm{ecs}} - V_{\mathrm{up}} - V_{\mathrm{rel}})V_{\mathrm{cell}}, \mu$l
P_{Ca}	0.25nA/mM	V_{up}	0.01
P_{CaK}	0.002	V_{rel}	0.1
P_{CaNa}	0.002	V_{SRup}	$V_{\mathrm{cell}} V_{\mathrm{up}} \mu$l
$[Ca^{2+}]_{\mathrm{o}}$	2mM	k_{mCa2}	625nA/mM
$[K^{+}]_{\mathrm{o}}$	4mM	M_{trop}	0.02mM
$[Na^{+}]_{\mathrm{o}}$	140mM	C_{trop}	0.05mM